OXFORD

Cerebral Cortex, 2022, 1–10
https://doi.org/10.1093/cercor/bhac273
Original Article

Transcranial magnetic stimulation to the angular gyrus modulates the temporal dynamics of the hippocampus and entorhinal cortex

Gillian Coughlan[1,2,*], Nichole R. Bouffard[1,3], Ali Golestani[3], Preston P. Thakral[4,5], Daniel L. Schacter[4], Cheryl Grady[1,6], Morris Moscovitch[1,3]

[1]Rotman Research Institute, Baycrest Health Sciences, 3560 Bathurst St, North York, Ontario M6A 2E1, Canada,
[2]Department of Neurology, Massachusetts General Hospital, Harvard Medical School, 15 Parkman St, Boston, MA 02114, United States,
[3]Department of Psychology, University of Toronto, 27 King's College Cir, Toronto, Ontario M5S 3G3, Canada,
[4]Department of Psychology, Harvard University, 33 Kirkland St, Cambridge, MA 02138, United States,
[5]Department of Psychology and Neuroscience, Boston College, 140 Commonwealth Ave, Chestnut Hill, MA 02467, United States,
[6]Department of Psychiatry, University of Toronto, 250 College Street, Toronto, Ontario M5T 1R8, Canada
*Corresponding author: Department of Neurology, Massachusetts General Hospital, Harvard Medical School, Boston, MA, United States. Email: gcoughlan@mgh.harvard.edu

Transcranial magnetic stimulation (TMS) delivered to the angular gyrus (AG) affects hippocampal function and associated behaviors (Thakral PP, Madore KP, Kalinowski SE, Schacter DL. Modulation of hippocampal brain networks produces changes in episodic simulation and divergent thinking. 2020a. *Proc Natl Acad Sci U S A*. 117:12729–12740). Here, we examine if functional magnetic resonance imaging (fMRI)-guided TMS disrupts the gradient organization of temporal signal properties, known as the temporal organization, in the hippocampus (HPC) and entorhinal cortex (ERC). For each of 2 TMS sessions, TMS was applied to either a control site (vertex) or to a left AG target region ($N = 18$; 14 females). Behavioral measures were then administered, and resting-state scans were acquired. Temporal dynamics were measured by tracking change in the fMRI signal (i) "within" single voxels over time, termed single-voxel autocorrelation and (ii) "between" different voxels over time, termed intervoxel similarity. TMS reduced AG connectivity with the hippocampal target and induced more rapid shifting of activity in single voxels between successive time points, lowering the single-voxel autocorrelation, within the left anteromedial HPC and posteromedial ERC. Intervoxel similarity was only marginally affected by TMS. Our findings suggest that hippocampal-targeted TMS disrupts the functional properties of the target site along the anterior/posterior axis. Further studies should examine the consequences of altering the temporal dynamics of these medial temporal areas to the successful processing of episodic information under task demand.

Key words: angular gyrus; functional connectivity; hippocampus; intervoxel and intravoxel pattern analysis; TMS.

Introduction

The temporal dynamics of the brain help us understand how it encodes information about the world at multiple scales. Distinctiveness or variability within neural gradients that exist along the axes of specific brain regions underlie this temporal organization and can be used to parcellate brain regions into distinct areas with specific functions (Fulcher et al. 2019; Spitmaan et al. 2020; El–Gaby et al. 2021). For example, the anteroposterior hippocampal gradient underlies memory acquisition, retention, and retrieval (Tambini and Davachi 2013; Brunec et al. 2018) by contributing to the hierarchical organization of memory from fine grained to gist-like encoding or retrieval of information (Poppenk and Moscovitch 2011; Poppenk et al. 2013; Robin and Moscovitch 2017; Grady 2019). Measuring neural gradients in humans has been made possible with recent advances in recording the properties of the functional magnetic resonance imaging (fMRI) signal over time. For example, the fMRI signal has been tracked with (i) single-voxel autocorrelation (i.e. the intravoxel similarity of single-voxel signals over time, AC) and (ii) intervoxel similarity (i.e. similarity between all regional voxel signals over time), both of which provide insights into the distribution of temporal dynamics across the neural gradient. Adopting such methods has allowed us to move beyond simply examining the anteroposterior axis of the human hippocampus (HPC), and opened up investigation of an anteromedial-posterolateral HPC division (Bouffard et al. in press) that was previously only seen in rodents (Jung et al. 1994; Hasselmo 2008; Kjelstrup et al. 2008; Komorowski et al. 2013; Igarashi et al. 2014). These methods give us greater insights into the organizational principles within the HPC, but we still do not know what cortical connections are associated with the functional properties of the medial temporal regions that support normal memory.

To investigate this, we focused on fMRI-guided transcranial magnetic stimulation (TMS) to the angular gyrus

Received: November 2, 2021. **Revised:** March 12, 2022. **Accepted:** March 15, 2022

(AG), a well-characterized component of the cortical-hippocampal network, on the basis of hypothesized interactions and functional connectivity between HPC and parietal cortex (Wagner et al. 2005; Kahn et al. 2008; Ritchey et al. 2015). For example, by applying magnetic TMS to the AG, we can alter hippocampal network connectivity and behaviors related to hippocampal function either positively (e.g. Wang et al. 2014; Freedberg et al. 2019) or negatively (Thakral et al. 2020). Thakral et al. (2020) recently showed that hippocampal-targeted TMS in the form of continuous θ-burst stimulation to the AG disrupts hippocampal network connectivity and subsequently hampers episodic simulation performance. Using the data from the Thakral et al. (2020) study, we ask: would perturbing the functional connections between HPC and AG via TMS also alter the temporal dynamics along the anterior/posterior axis of the human HPC, and, if so, would these alterations be related to functional connectivity of the HPC to neocortex?

We first set out to characterize the temporal organization of subdivisions within the bilateral HPC and entorhinal cortex (ERC) under a control TMS condition (i.e. following application of TMS to the vertex). This was achieved by means of a data-driven clustering approach, which moves beyond a simple parcellation of hippocampal and entorhinal subdivisions by means of anatomical masks. We included the ERC because the main interface between the HPC and higher association areas of the cortex is the ERC. We then examined the effect of TMS on temporal organization of these regions unilaterally, using two techniques: single-voxel autocorrelation and intervoxel similarity. As the left anterior HPC is the main target of this modulation, we expected that TMS would reduce functional connectivity between AG and the left anterior HPC compared with the control TMS condition and that the temporal dynamic in the left anterior HPC would be altered compared with the control TMS condition. We hypothesized that of the two metrics used, single-voxel autocorrelation may be more sensitive to TMS than intervoxel similarity, as prior studies have shown that intravoxel autocorrelation is more sensitive to external manipulations (e.g. a task) than intervoxel similarity (Brunec et al. 2018).

Materials and methods

Participants, procedure, and MRI acquisition

This study included 18 young, healthy individuals (21.6 ± 1.6 years old; 10 females). Informed consent was obtained from all participants prior to participation, with protocol approval from the Institutional Review Board of Harvard University. All participants self-reported to be native English speakers and right-handed, with normal or corrected-to-normal vision. Details of the MRI acquisition and TMS procedures are described in Thakral et al. (2020). TMS that evokes long-lasting (i.e. ~60 min) effects in the form of continuous θ-burst stimulation was applied to the control site (vertex) or the left AG on different days in a counterbalanced order. Following application of TMS and a series of functional tasks, including an episodic simulation task based on visual word cues, a resting-state scan was acquired. The resting-state scan was collected ~25 min after TMS and was the focus of the current investigation. The left AG TMS target was identified on the basis of a participant-specific functional connectivity analysis (i.e. a seed-to-voxel analysis) from a resting-state scan acquired where no TMS was delivered, with the left anterior HPC as the seed (coordinate of $x = -25$, $y = -10$, and $z = -19$; Wu et al. 2015). Resting-state images were acquired with a multiband echo-planar imaging sequence (time repetition, TR of 650 ms, time echo, TE 34.80 ms, matrix size of 90 × 90, 64 slices [8 slices acquired simultaneously], and 2.3-mm^3 resolution).

MRI data were preprocessed using a pipeline written in bash, which incorporated several tools from the FMRIB Software Library (FSL, Oxford; Smith et al. 2004). Preprocessing was conducted with "MELODIC" (multivariate exploratory linear optimized decomposition into independent component, Beckmann 2012) to remove artifacts such as motion, CSF signal, white matter signal, as well as physiology and scanner artifacts. This included removal of the first 5 volumes (to account for signal steady-state transition and T_1w equilibration), slice timing correction, and head motion correction. To spatially normalize the functional EPI image, the T_1w images were used to register the functional data to their corresponding anatomical images, and the resulting aligned T_1w dataset was transformed into MNI space. Functional images were resampled to 2 mm^3 and spatially smoothed using a 4-mm full-width half-maximum (FWHM) Gaussian kernel. To correct for low-frequency drifts, we applied temporal high-pass filtering (100 s or 0.01 Hz). Given the modest sample size, automated de-noising approaches such as FIX and AROMA were not appropriate.

Protocol for TMS manipulation

The TMS protocol was composed of 50-Hz triplets (3 single pulses separated 8 by 20 ms) repeated at a frequency of 5 Hz (every 200 ms) for a duration of 40 s (or 600 pulses) using parameters from Huang et al. (2005) This TMS protocol was assumed to be inhibitory and was expected to impair performance (Thakral et al. 2020). Continuous theta burst stimulation (cTBS) intensity was determined from the participant-specific motor threshold. In this procedure, the left motor cortex was identified on each participant's anatomic image and motor threshold was defined as the lowest single-pulse TMS intensity that produced 5 out of 10 motor responses in the right hand namely, visual detection of a finger twitch in the right hand; motor threshold was set at 70% of stimulator output if no twitch was evident at this intensity. Once identified, cTBS intensity was set at 90% of the resting motor threshold of 60.73. In contrast to repeated TMS, cTBS disrupts neural activity with shorter TMS durations, namely, 40 s relative to 60 min of 1 Hz TMS, which would

produce roughly equivalent durations of inhibitory TMS effects. Therefore, for reasons of participant comfort and overall feasibility, a cTBS as opposed to repeated TMS protocol was adopted.

Statistical analysis

Single-voxel autocorrelation

We used data-driven clustering of single-voxel autocorrelation to discover potentially novel organizations of neural distinctiveness along both the bilateral HPC and ERC axes. This included a bilateral analysis as we wanted to confirm that the temporal organization of the HPC and ERC axes were similar by hemisphere. We calculated the autocorrelation of individual voxels, to isolate as small an area of each structure as possible. HPC and ERC masks were generated using the Harvard-Oxford Atlas in FSL (v6.0.0) and the timeseries for each voxel in each structure was extracted for both fMRI runs (i.e. following TMS to the vertex and AG) using niftiread in MATLAB (2018). The degree of similarity between a voxel's signal and the temporally shifted version of the signal was measured over 650-ms time intervals, 5 times in total. The total duration of 3,200 ms was chosen based on evidence that the resting-state autocorrelation is very close to zero after 4 s, following preprocessing (Bollmann et al. 2018; Chen et al. 2019). Applying this procedure resulted in 5 single-voxel autocorrelation values representing each shift, allowing us to assess the signal similarity over time within a single voxel. Autocorrelation values were z scored by subtracting the mean and dividing by the standard deviation across voxels within each mask, so that meaningful comparisons could be made between regions.

We then applied the Louvain clustering method on the extracted single-voxel autocorrelation values (5 values per voxel based on 5 shifts), within the bilateral ERC and HPC separately, for both the vertex and AG TMS conditions. Thus, there were no pre-specified AC threshold values. The Louvain clustering method was originally developed to detect communities based on neural similarity. Here, we used this approach to extract autocorrelation clusters based on the 5 single-voxel autocorrelation vector values. The Euclidean distance between the autocorrelation of each pair of neighboring voxels was calculated to create a distance matrix. This similarity matrix was used to generate regional clusters using the algorithm (Blondel et al. 2008; Wickramaarachchi et al. 2014). In addition to clustering at the level of each individual in both TMS fMRI runs, we created group cluster maps in the vertex control condition averaged across the 18 study participants to investigate whether the community clusters fall in the same anatomical location as the expected neural subdivisions of the HPC and ERC axes. We used the Jaccard similarity index (also known as Jaccard similarity coefficient) to measure the amount of spatial overlap between clusters, giving us an anatomically consistent percentage across participants. Coefficients can range from 0% to 100%, with a higher percentage reflecting more consistent clusters across participants. Average single-voxel autocorrelation was then submitted to a repeated-measure analysis of variance (ANOVA) with subdivision (generated clusters) and TMS condition (AG vs vertex) as factors. Given the apriori hypothesis as it relates to AG TMS effects on the anterior-medial HPC, we did not correct for multiple comparisons. We also tested whether correlations between regional subdivisions differed by TMS condition, using Fisher *r*-to-*Z* transformed rs (ZPF), which tests for the difference between two nonindependent correlations and differs from the *Z* test for the difference between independent correlations by the adjustment factor (Raghunathan et al. 1996).

Finally, as temporal signal-to-noise ratio (SNR) may interfere with the estimation of the autocorrelation of the fMRI signal, we aimed to rule out the possibility that the hippocampal and entorhinal autocorrelation subdivisions are being driven by fMRI noise. We thus calculated the temporal SNR for each subdivision and tested whether the hippocampal autocorrelation could be explained by temporal SNR. The results of this analysis showed that SNR could not explain our primary results and are found in the Supplementary Materials.

Intervoxel similarity

Next, we applied the group level regional subdivision (i.e. cluster) masks generated using the single-voxel autocorrelation method. Our aim was to assess if intervoxel similarity (i.e. the similarity in signal from spatially separable voxels) of our HPC and ERC subdivisions of interest differed in terms of their mean intervoxel similarity. Such a finding would suggest that temporal dynamics along the axes can be defined by intervoxel similarity as well as single-voxel autocorrelation. Voxelwise activity estimates were standardized. We calculated the Pearson correlations between each pair of voxels per mask, which was then *r* to z transformed. Average estimates of similarity were derived leaving only one estimate of similarity between every pairwise combination of voxels, which were then averaged to produce an overall estimate of intervoxel similarity. These estimates, along with the average single-voxel autocorrelation, were then submitted to a repeated-measure ANOVA with subdivision and TMS condition as factors.

Functional connectivity

Functional connectivity between the left HPC subdivisions (generated using single-voxel autocorrelation clustering) and the left AG target was analyzed by extracting the first eigenvector from the blood oxygen level–dependent (BOLD) timeseries for each regions of interest, and each single participant, using "fslmeants." This timerseries was used to determine whether functional connectivity between AG and the anterior division of the HPC (i.e. the target region) was reduced following TMS to the AG compared with the vertex, consistent with Thakral et al. (2020). A simple linear regression model

was also applied to test whether the pattern of functional connectivity change (vertex—AG condition) between the left AG and the TMS target site predicted change in the single-voxel autocorrelation in the TMS target site.

Episodic simulation behavioral measure

Participants also completed a post-scan interview in which they re-viewed the object word cues that had been shown during scanning and were instructed to report verbally what they had thought about for each cue during the episodic simulation task. During scanning, participants covertly imagined a novel and specific future episode using the cue as a starting point. Responses were audio-recorded and transcribed for analysis (see Thakral et al. 2020 for further details). Each future event was scored in accordance with the Autobiographical Interview (Levine et al. 2002) and assessed for both internal (episodic) and external (non-episodic) details. These behavioral data were included in the analysis for exploratory purposes as a secondary aim to determine if altered functional organization along the HPC and ERC axes correlated with TMS-related deficits in memory performance.

Results

Our first analysis examined the location and consistency of single-voxel autocorrelation clusters (subdivisions) along the HPC and ERC axes, in the vertex control fMRI run. We then compared average autocorrelation values of the generated subdivisions to confirm that mean subdivision values significantly differed from one another. In order to validate the vertex condition as our control condition, we assessed whether the location of single-voxel autocorrelation clusters overlapped with those identified by Bouffard et al. (in press), who implemented the same data-driven parcellation in a resting fMRI run without TMS. Next, we examined the effects of TMS on the autocorrelation clusters along the HPC and ERC axes to examine if changes in AG connectivity as a function of TMS condition, namely, vertex relative to AG, modulates single-voxel autocorrelation. Such a result would suggest that AG connectivity modulates temporal dynamics along the HPC and ERC axes.

Temporal organization of HPC and ERC axes

The group cluster map based on the resting-state data collected following TMS to the vertex revealed subdivisions along the axes, with high single-voxel autocorrelation clusters situated in the anteromedial HPC and the posteromedial ERC consistent with Bouffard et al. (in press). The low single-voxel autocorrelation clusters were situated in the posterolateral HPC and the anterolateral ERC (Fig. 1A). Note that for the HPC only; an intermediate autocorrelation cluster was also generated. Using Jaccard's coefficient, we compared the consistency of the cluster locations across participants in the vertex condition, by calculating the amount of overlap across the participants. This analysis revealed 43–58% overlap of HPC and ERC cluster locations across all participants in both hemispheres. In contrast, the location of the intermediate HPC cluster showed only 10–13% overlap or consistency in its location across participants. Given the significant variability of this cluster's location across participants in our sample, and the fewer voxels it contained, it was not retained for TMS analyses. Please refer to Table 1 for the mean single-voxel autocorrelation values.

Effects of TMS on functional connectivity and single-voxel autocorrelation along the left HPC and ERC axes

We first confirmed that following TMS to the AG there was reduced functional connectivity between the left AG and the target anterior division of the left HPC (characterized above with the single-voxel autocorrelation clustering method). There was a significant reduction in connectivity between left AG and the left anteromedial HPC following TMS to the AG (Mean: 0.456; SD: 0.205) relative to the vertex (Mean: 0.551; SD: 0.178; $t = -1.97$, $df = 17$, $P = 0.042$, Cohen's $d = 0.48$). Connectivity with the left posterolateral HPC was not affected by stimulation, nor was AG connectivity with either of the ERC subdivisions (P's > 0.15).

We next investigated the effect of TMS to the left AG on (i) single-voxel autocorrelation and (ii) intervoxel similarity along the neural gradient of the left HPC and ERC axes presented in Fig. 1A. We were interested in whether AG stimulation altered the autocorrelation of the target site, such that the mean autocorrelation was reduced in the anteromedial HPC following TMS to the AG relative to the vertex.

Single-voxel autocorrelation

A 2-way repeated-measure ANOVA model assessing the effects of subdivision and TMS condition (AG and vertex) revealed a main effect of TMS condition on the left HPC axis ($F(1,17) = 5.67$, $P = 0.025$; $\eta_p^2 = 0.261$), with no TMS condition × HPC cluster interaction ($P = 0.854$). Although the interaction was not significant, paired-sample t-tests were utilized to evaluate the effect of TMS condition on the 2 subdivisions independently to investigate if the effect of TMS specifically altered the autocorrelation of the anteromedial HPC, as expected from the results of Thakral et al. (2020). TMS to the AG relative to the vertex significantly decreased the mean single-voxel autocorrelation of the anteromedial HPC ($t = -2.453$, $df = 17$, $P = 0.025$; Cohen's $d = 0.50$), but did not significantly decrease single-voxel autocorrelation in the posterolateral HPC ($P = 0.097$; see Fig. 2B). Pearson correlations further showed that following AG TMS, single-voxel autocorrelation measures in the 2 clusters were significantly correlated with one another ($r = 0.662$, $P = 0.001$), unlike in the vertex TMS condition ($r = 0.176$, $P = 0.437$). Correlations differed by TMS condition (ZPF = 1.692, 1-tailed $P = 0.045$), suggesting that normal variability of temporal dynamics along the long

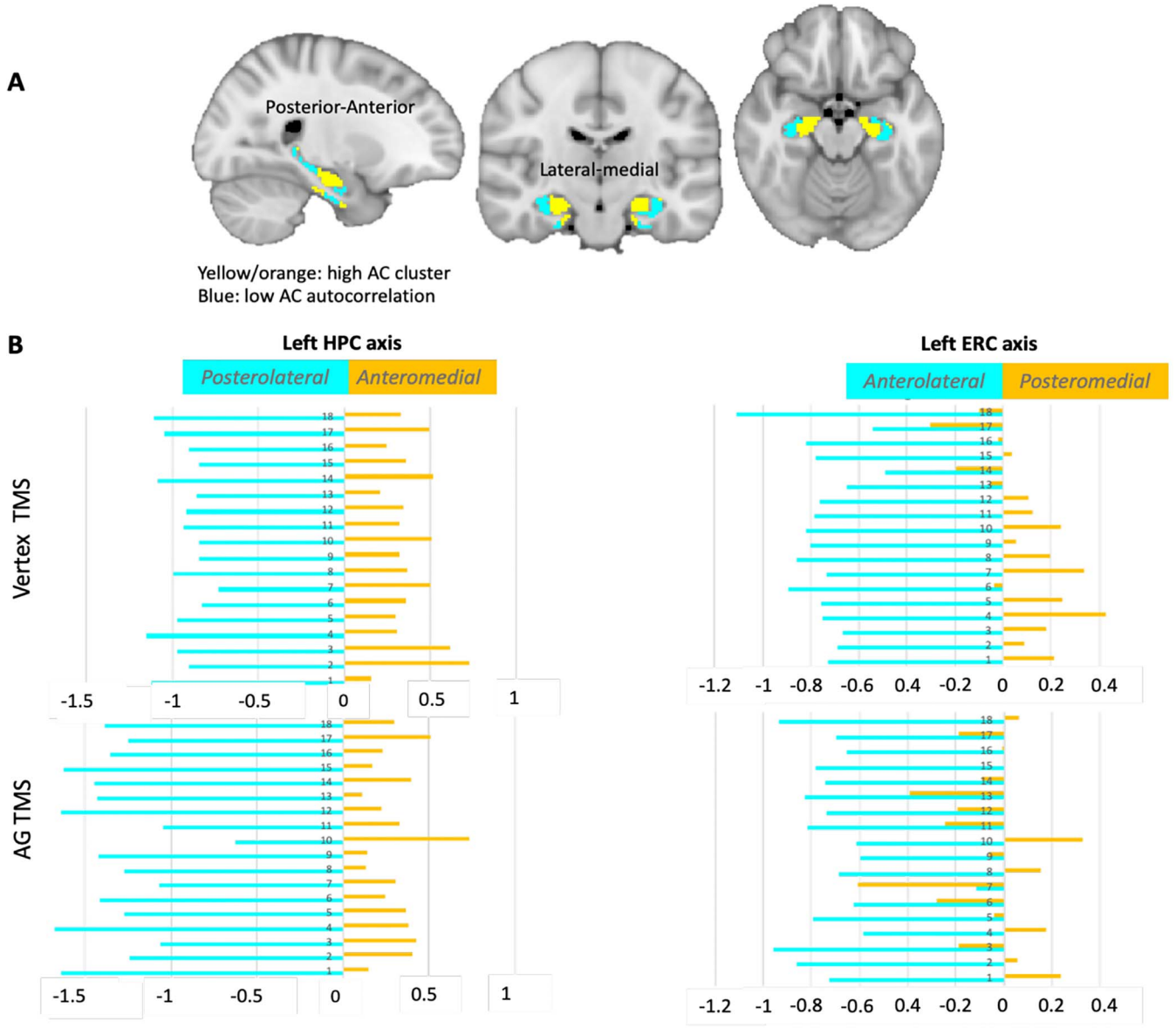

Fig. 1. Temporal organization along the HPC and ERC axes generated using Louvain clustering on the autocorrelation of a single-voxel timecourses. A) Group-average clusters generated by averaging the similarity matrices across all participants. Blue: low single-voxel autocorrelation cluster yellow: high single-voxel autocorrelation cluster. First, we identified divisions of the HPC and ERC based on the amount of single-voxel autocorrelation in the BOLD-signal on an intravoxel level. B Individual effects ($n = 18$) of TMS to the vertex (top row) and AG (bottom row) on the single-voxel autocorrelation (illustrated along the *x* axis; see next section for statistical effects). Blue: low single-voxel autocorrelation division (fMRI signal from any given voxel is variable and not correlated with itself over time). Yellow/orange: high single-voxel autocorrelation division (fMRI signal from any given voxel is highly correlated with itself over time). Z-transformed values are presented since the relative autocorrelation values in subdivisions was the metric interest (over raw absolute values).

axis of the HPC was reduced in the AG TMS condition. Individual effects of TMS (AG vs vertex) on the single-voxel autocorrelation are presented in Fig. 1B. Finally, we tested whether reduced functional connectivity between the left AG and the anteromedial HPC predicted reduced single-voxel autocorrelation in the anteromedial HPC specifically, as this was the AG TMS target site. As expected, a simple linear regression showed that reduced functional connectivity was associated with lower single-voxel autocorrelation in the anteromedial HPC ($F(1,17) = 6.736$, $P = 0.020$; Fig. 2C), but not the posterolateral HPC ($F(1,17) = 0.488$, $P = 0.495$).

Along the axis of the ERC, there was a main effect of TMS condition on the left ERC ($F(1,17) = 8.265$, $P = 0.011$, $\eta_p^2 = 0.341$), as well as a significant TMS condition x ERC cluster interaction ($F(1,17) = 4.576$, $P = 0.048$, $\eta_p^2 = 0.222$), which revealed that the mean single-voxel autocorrelation of the posteromedial division was significantly decreased following TMS to the AG relative to the vertex ($t = 2.78$, $df = 17$, $P = 0.013$, Cohen's $d = 0.652$), whereas the mean autocorrelation of the anterolateral division did not change ($P = 0.277$; Fig. 2D). Pearson correlations further showed that following AG TMS, the ERC clusters were significantly correlated with

Table 1. Summary of the statistical effects.

Regional subdivision (i.e. cluster)	TMS stimulation condition	Mean single-voxel autocorrelation	TMS condition main effect statistics	Subdivision × TMS stimulation statistics
Left HPC axis				
Anteromedial	Vertex	0.386 ± 0.146	$P = 0.025^*$ ($F = 6.02$)	$P = 0.854$ ($F = 0.37$)
	AG	0.309 ± 0.157		
Posterolateral	Vertex	−0.949 ± 0.118	$P = 0.091$ ($F = 3.08$)	
	AG	−1.02 ± 0.169		
Left ERC axis				
Posteromedial	Vertex	0.133 ± 0.122	$P = 0.013^*$ ($F = 7.24$)	$P = 0.032^*$ ($F = 5.21$)
	AG	−0.038 ± 0.168		
Anterolateral	Vertex	−0.672 ± 0.158	$P = 0.277$ ($F = 2.12$)	
	AG	−0.613 ± 0.088		

Note: Effects of TMS on the single-voxel autocorrelation within subdivisions of the left HPC and ERC. HPC: HPC; entorhinal cortex: ERC; transcranial magnetic stimulation: TMS; interaction: X. *denotes significance

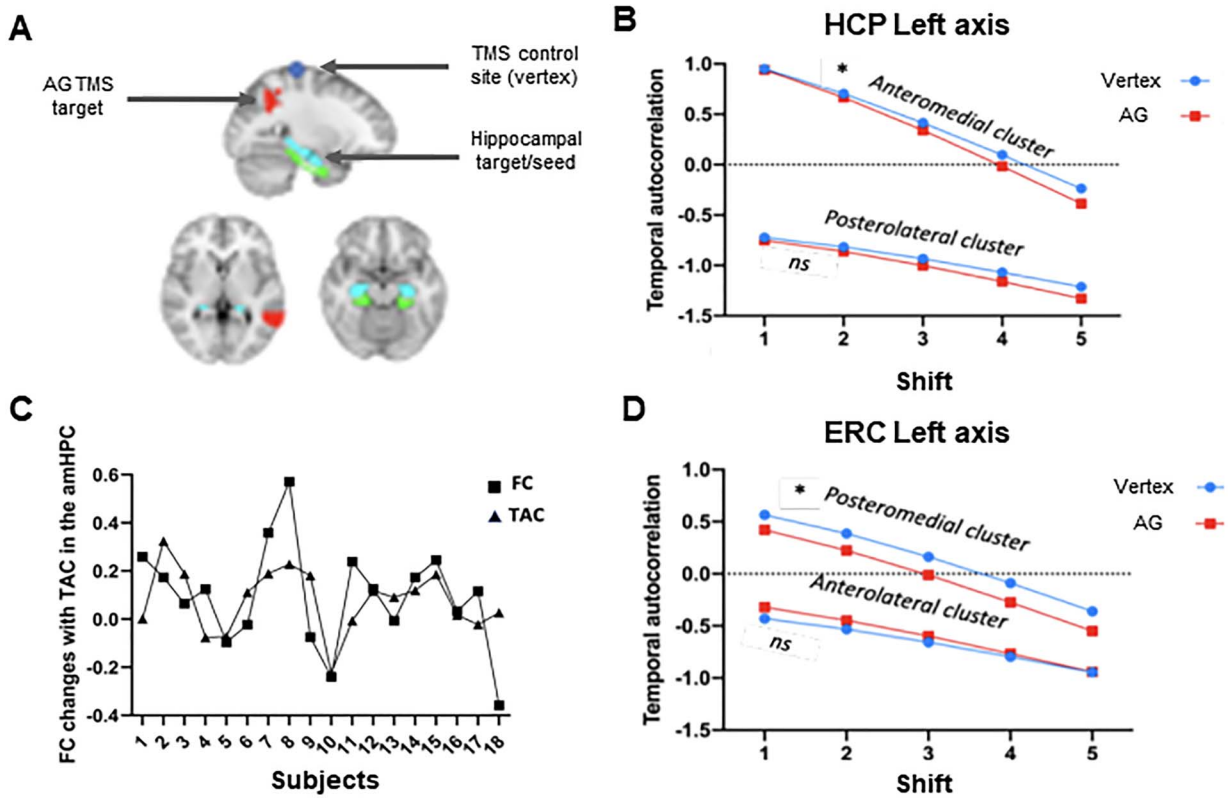

Fig. 2. Experimental design and TMS effects on the single-voxel autocorrelation along the HPC and ERC axes. A) Before participants entered the scanner, TMS was applied to the control site (vertex) or the left AG target on different days. The AG target was identified on the basis of a resting-state functional connectivity analysis (i.e. a seed-to-voxel analysis) with the left anterior HPC as the seed when no TMS was applied (red indicates squares that illustrate the individualized AG TMS targets). B) Significant main effect of stimulation on the left anteromedial HPC, wherein TMS significantly decreased the mean single-voxel autocorrelation. C) Significantly reduced functional connectivity (FC; vertex—AG) predicts reduced single-voxel autocorrelation (TAC; vertex—AG) in the targeted anteromedial division of the HPC. D) Significant main effect of stimulation on the AC of the left posteromedial ERC, with a significant stimulation x subdivision interaction. Shift: the degree of similarity between a timeseries and the temporally shifted version of the timeseries was measured over 650-ms time intervals, 5 times in total. This resulted in 5 single-voxel autocorrelation values for each regional voxel representing each shift, illustrated along the x axis of B) and D).

one another ($r = -.519$, $P = 0.033$) (left hemisphere only), unlike following TMS to the vertex ($r = -.023$, $P = 0.241$), with a significant difference between correlations (ZPF =1.728, 1-tailed $P = 0.041$). Thus, both the HPC and ERC results indicate that TMS resulted in reduced single-voxel autocorrelation differences between the subdivisions of these structures (i.e. a less differentiated neural gradient). See Table 1 for a summary of the TMS effects and mean single-voxel autocorrelation cluster values.

Results for the right HPC and right ERC as non-targeted regions are detailed in the supplementary materials (see Supplementary Table 1 and Supplementary Figs. 1 and 2).

Intervoxel similarity

A two-way repeated-measure ANOVA model with factors subdivision and TMS condition, showed that there was a main effect of subdivision along the left HPC axis, with higher intervoxel similarly in the anteromedial compared with the posterolateral subdivision ($F = 69.54$,

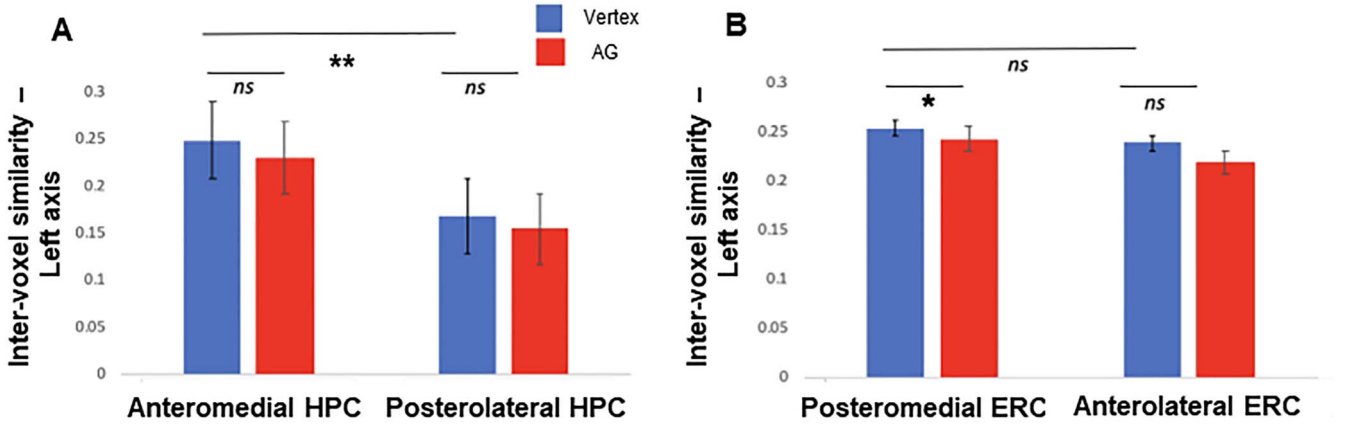

Fig. 3. Effects on the intervoxel similarity along the HPC and ERC axes as a function of TMS condition (vertex and AG) and Louvain clustering generated subdivision. A) Main effect of subdivision on intervoxel similarity, but no effect of TMS along the HPC axis. Like the pattern single-voxel temporal autocorrelation, intervoxel similarity is higher in the anteromedial division and lower in the posterolateral division of the left HPC. B) Main effect of stimulation on intervoxel similarity across the ERC axis. No main effect of subdivision on intervoxel similarity.

Table 2. Intervoxel similarity and single-voxel autocorrelation.

		Autocorrelation AM HPC	Autocorrelation PL HPC
Intervoxel PL HPC	Pearson R	−0.079	0.267
Intervoxel AM HPC	Pearson R	−0.127	0.277
		Autocorrelation PM ERC	Autocorrelation AL ERC
Intervoxel PM ERC	Pearson R	0.298	−0.398
Intervoxel AL ERC	Pearson R	0.011	−0.148

Note: Pearson correlation showed that these measures are not correlated. HPC: HPC; ERC: Entorhinal cortex; AM: Anteromedial; PM: Posteromedial; AL: Anterolateral. PL: Posterolateral.

$P = 0.000$, and $np^2 = 0.804$). There was no effect of TMS condition on the mean intervoxel similarity of the HPC axis ($P = 0.348$), and no TMS × HPC subdivision interaction ($P = 0.760$ Fig. 3A). In contrast, there was no main effect of subdivision on intervoxel similarity along the left ERC axis ($P = 0.117$), but there was a main effect of TMS condition along the ERC axis ($F(1,17) = 4.36$, $P = 0.043$, $np^2 = 0.220$; Fig. 3B). Mean values showed that TMS to the AG relative to the vertex decreased the overall intervoxel similarity along the left ERC. The TMS condition × ERC subdivision interaction, however, was not significant ($P = 0.518$). Results for the right HPC and ERC are detailed in the Supplementary Materials.

Based on the above set of results, the single-voxel autocorrelation along the HPC and ERC axes was more sensitive to TMS than intervoxel similarity. We thus examined the relation between single-voxel autocorrelation and intervoxel similarity following TMS to the vertex, since evidence exists that these two metrics relate differently to behavior (Brunec et al. 2018). Indeed, these measures were not correlated with one another (Table 2), suggesting that the intravoxel vs intervoxel signals may tap into dissociable neural characteristics along the HPC and ERC axes.

Episodic simulation and the temporal dynamics in HPC and ERC following TMS

Thakral et al. (2020) found no significant relation between functional connectivity at-rest and behavior. Nevertheless, in an exploratory analysis, we used a univariate ANOVA to test whether within-subject mean single-voxel autocorrelation change in each subdivision of either structure (4 in total) following TMS to the AG and vertex predicted declines in episodic simulation performance between the two TMS conditions as measured by the number of episodic details generated. We focused on single-voxel autocorrelation because this metric was more vulnerable to the effects of TMS than intervoxel similarity (see above). None of the brain predictor variables had a significant effect on measures of episodic simulation performance.

Discussion

We found that TMS to the left AG that targeted the left anterior HPC, compared with TMS to a control site, altered the single-voxel autocorrelation of the anteromedial HPC and posteromedial ERC, both of which were in a high state of autocorrelation in the vertex condition. The axial divisions in the vertex control condition followed the divisions reported by Bouffard et al. (2023), who implemented the same data-driven clustering method in a non-TMS fMRI run, suggesting that the vertex condition used here reflects the temporal dynamics across the axis of the HPC and ERC in their natural state. Functional connectivity between the anteromedial HPC and AG was reduced following TMS, and this pattern of functional connectivity change was correlated with single-voxel autocorrelation change in the same subdivision of the HPC. Thus, intact hippocampal

connectivity with the left inferior parietal lobule appears to be associated with sustaining neural distinctiveness along the axis, which in turn help characterizes its organization. Interestingly, TMS had no noticeable effect on organization measured by intervoxel similarity in the HPC.

As expected, we observed evidence of temporal dynamics along the HPC and ERC axes, which has been previously documented in rodents (Jung et al. 1994; Hasselmo 2008; Kjelstrup et al. 2008; Komorowski et al. 2013) and in one human study to date (Bouffard et al. 2023) that used the same clsutering method reported in this study. Specifically, the anteromedial HPC and the posteromedial ERC demonstrated higher single-voxel autocorrelation and a slower changing signal over longer timescales. In turn, the posterior-lateral HPC and anterior-lateral ERC demonstrated lower single-voxel autocorrelation and a faster changing signal at shorter timescales. This organizational pattern is consistent with rodent models showing that the temporal dynamics of the HPC is characterized by greater firing stability of neurons over time in the anteromedial HPC compared with the posterolateral HPC (Jung et al. 1994; Hasselmo 2008; Kjelstrup et al. 2008; Komorowski et al. 2013). This HPC and ERC distinctiveness between subdivisions may then support coarse-to-fine grained representational scales, although the former is anterior to posterior, whereas the latter is posterior to anterior.

Building on this observation, we also found that the intervoxel similarity follows the same temporal characterization along the HPC axis, but not along the ERC axis. Reasons for the inconsistency between the single-voxel autocorrelation and intervoxel similarity along the ERC may include (i) not enough statistical power in a sample of 18 participants to detect temporal dynamics along the relatively short axis of the ERC using a cruder measure of temporal dynamics such as intervoxel similarity and (ii) the single-voxel autocorrelation and intervoxel similarity measures capture separable aspects of representational encoding, as suggested by Brunec et al. (2018).

Hippocampal-targeted TMS reduced the single-voxel autocorrelation along the long axis of the HPC. The ERC and HPC subdivisions that had characteristically higher single-voxel autocorrelation at control (i.e. vertex stimulation) were most vulnerable to TMS to the left AG (i.e. the posteromedial ERC and the anteromedial HPC). This finding suggests that compromised AG connectivity co-occurs with disrupted organizational firing of broad cell ensembles, reducing the inherent distinctiveness in neuronal firing along the axes, which may be necessary for optimal functioning (Poppenk et al. 2013). Supporting this interpretation, autocorrelation values in the regional subdivisions became highly correlated following TMS to the AG, but not the vertex. The organization of the ERC, from where the HPC receives its inputs, was also altered such that subdivisions showed less distinctive autocorrelation following TMS. However, ERC connectivity to AG was not affected by AG TMS. Future studies should thus examine whether autocorrelation changes in the ERC influence temporal dynamics in the HPC or vice versa.

Interestingly, intervoxel similarity along the HPC axis was not modulated by AG TMS stimulation. Brunec et al. (2018) also found no modulation of intervoxel similarity along the HPC axis in response to navigational task difficulty, though there was modulation of single-voxel autocorrelation along the HPC axis. Thus, TMS may impact the signal stability (i.e. autocorrelation) of large cell populations in a similar way, so that the relation between voxels (intervoxel similarity) would not change following stimulation. That is, if the cells in anteromedial HPC are all changing their autocorrelation in a similar way due to TMS, the correlation between a given cell's activity pattern and that of its neighbors would not differ compared with control. Alternatively, the absence of an effect on intervoxel similarity may suggest that signal complexity between voxels within the HPC is resistant to fluctuations from the inferior parietal cortex, unlike the temporal shifting patterns within-voxels. Whatever the interpretation, both metrics may tap into dissociable HPC functions.

Our single-voxel autocorrelation measure may relate to spatially and temporally organized traveling waves that are characterized by theta and alpha oscillations observed in the HPC and the cortex (Zhang et al. 2018; Lubenov et al. 2009). Zhang et al. (2018) show that theta and alpha oscillations cluster to form spatial phase gradients at frequencies (2–15 Hz) that are higher than what is achieved with fMRI (~0.01–0.1 Hz). These oscillatory clusters (measured via direct brain recordings during neurosurgery) propagate in a posterior-to-anterior direction in a similar fashion to the autocorrelation clusters on BOLD-signal reported here. Behaviorally, the direction of oscillations is related to episodic memory. We did not detect a brain-behavioral association on the autocorrelation derived from the resting-state BOLD-signal, which may in part be due to the low-frequency band that characterizes the BOLD-signal. The high temporal resolution may provide stronger/more robust autocorrelation readouts due to this density of electrocorticographic data.

There are limitations of this work and recommendation for future research. First, there is evidence that local field potentials are correlated with fMRI signals (Logothetis et al. 2001; Killian et al. 2012; Strange et al. 2014), but the spatial resolution of fMRI is much coarser then that of invasive recordings. Today, most studies comprise voxel volumes of 8–30 mm^3 (isotropic voxel with side length 2–3 mm), including 10^5–10^6 neurons (Vanni et al. 2015). The single- voxel autocorrelation and intervoxel similarity of the BOLD-signal, therefore, captures the behavior of populations of neurons. It would be interesting to know how the behavior of these populations relate to the behavior of single neurons. Future investigations should aim to replicate these findings in rodent studies (Strange et al. 2014) and in humans (Quiroga, 2019). Although no brain-behavior relation was found, we expect single-voxel autocorrelation during task demand

or with a larger sample size will be related to behavior, as shown by Bouffard et al. (2023). TMS may also have effects on regions outside the inferior parietal cortex and medial temporal lobe, such as on resting-state networks including the frontoparietal control network and the visual attention network (Freedberg et al. 2019; Thakral et al. 2020). Here, we highlighted the findings pertaining to the HPC given strong experimental work demonstrating that AG TMS affects normal hippocampal function. In the future, we hope to extend this analysis to other regions.

It is notable that resting-state functional connectivity change between the left AG and anteromedial HPC co-occurred with organizational changes that were most notable in the anteromedial HPC and posterolateral ERC. It is still unknown, however, whether (i) AG TMS reduces this functional connectivity with negative consequences for the organization of neurons in the HPC and ERC or (ii) disruption to the organization of HPC and ERC neurons leads to reduced hippocampal connectivity with the AG. Understanding the causal pattern of effects will aid our understanding of the role of neural gradients and their organization, in terms of their contribution to functional connectivity patterns between the memory dependent regions of the medial temporal lobe and the cortex. Finally, AG TMS did not appreciably alter intervoxel similarity within the anteromedial HPC relative to vertex TMS. This may suggest that there are at least two types of hierarchical organization, but further research comparing these temporal (within-voxel) and spatial (between-voxel) autocorrelation techniques are needed before such assumptions can be drawn.

TMS affected higher mean single-voxel autocorrelation in the more anterior division of the HPC. In line with this finding, previous research shows that the anterior HPC is more involved in encoding than the posterior HPC (Schacter and Wagner 1999; Kim 2015; Grady 2019; Fritch et al. 2020), suggesting that the natural state of the anterior division is for high single-voxel autocorrelation and a bias for encoding. Thus, AG TMS may alter episodic encoding of new information but have less impact on retrieval processes, which may rely on faster temporal changes in the posterior division. More research is needed to test this hypothesis.

In conclusion, our findings provide novel evidence that TMS to the inferior parietal cortex modulates the temporal dynamics of the HPC and ERC axes. Specifically, temporal dynamics in the anteromedial HPC and posteromedial ERC shifted more rapidly between successive time points (lowering the single-voxel autocorrelation) following TMS to the inferior parietal lobe. This effect was concentrated in these two axial subdivisions that show higher signal stability (or higher single-voxel autocorrelation) and led to a reduction in differentiation along the axes that we know traditionally supports optimal memory and navigation. The combination of TMS and temporal dynamics used here to map neural distinctiveness that characterizes the organization of brain regions, opens new ways to investigate the organization of the HPC and related structures, their functional interaction with neocortex, and their relation to behavior.

Supplementary material

Supplementary material is available at *Cerebral Cortex* online.

Authors' contributions

M.M., C. G, D.S., and P.T. designed the experiment. D.S. and P.T. performed the experiments. G.C. wrote the first draft. All authors substantially revised the manuscript. A.G. contributed with the software. G.C. and C.G. analyzed the data and all authors contributed to interpretation of results. All authors have read and approved the manuscript.

Funding

This work was supported by a Postdoctoral Fellowship Award from the Alzheimer's Society of Canada (award number 22-08 to G.C.), a Foundation Grant from Canadian Institutes of Health Research (grant number MOP-143311 to C.G.), Discovery grant from Natural Sciences and Engineering Research Council of Canada (grant number A8347 to M.M.), and by a grant from the National Institute of Mental Health (grant number R01 MH60941 to D.S.).

Conflict of interest statement: The authors declare no competing financial interests.

References

Beckmann CF. NeuroImage modelling with independent components. *NeuroImage*. 2012:62:891–901.

Blondel VD, Guillaume JL, Lambiotte R, Lefebvre E. Fast unfolding of communities in large networks. *J Stat Mech Theory Exp*. 2008:2008.

Bollmann S, Puckett AM, Cunnington R, Barth M. Serial correlations in single-subject fMRI with sub-second TR. *NeuroImage*. 2018:166:152–166.

Bouffard et al. 2023. Single voxel autocorrelation uncovers gradients of temporal dynamics in the hippocampus and entorhinal cortex during rest and navigation. *Cereb Cortex*. Forthcoming.

Brunec IK, Bellana B, Ozubko JD, Man V, Robin J, Liu ZX, Grady C, Rosenbaum RS, Winocur G, Barense MD, et al. Multiple scales of representation along the hippocampal anteroposterior Axis in humans. *Curr Biol*. 2018:28:2129–2135.e6.

Chen JE, Polimeni JR, Bollmann S, Glover GH. On the analysis of rapidly sampled fMRI data. *NeuroImage*. 2019:188:807–820.

El-Gaby M, Reeve HM, Lopes-dos-Santos V, Campo-Urriza N, Perestenko PV, Morley A, Strickland LAM, Lukács IP, Paulsen O, Dupret D. An emergent neural coactivity code for dynamic memory. *Nat Neurosci*. 2021:24.

Freedberg M, Reeves JA, Toader AC, Hermiller MS, Voss JL, Wassermann EM. Persistent enhancement of hippocampal network connectivity by parietal rTMS is reproducible. *eNeuro*. 2019:6:1–13.

Fritch HA, MacEvoy SP, Thakral PP, Jeye BM, Ross RS, Slotnick SD. The anterior hippocampus is associated with spatial memory encoding. *Brain Res*. 2020:1732:146696.

Fulcher BD, Murray JD, Zerbi V, Wang XJ. Multimodal gradients across mouse cortex. *Proc Natl Acad Sci U S A*. 2019:116:4689–4695.

Grady CL. Meta-analytic and functional connectivity evidence from functional magnetic resonance imaging for an anterior to posterior gradient of function along the hippocampal axis. *Hippocampus*. 2019:30:456–471.

Hasselmo ME. Grid cell mechanisms and function: contributions of entorhinal persistent spiking and phase resetting. *Hippocampus*. 2008:18:1213–1229.

Huang YZ, Edwards MJ, Rounis E, Bhatia KP, Rothwell JC. Theta burst stimulation of the human motor cortex. *Neuron*. 2005:5(2): 201–206.

Igarashi KM, Ito HT, Moser EI, Moser MB. Functional diversity along the transverse axis of hippocampal area CA1. *FEBS Lett*. 2014:588: 2470–2476.

Jung MW, Wiener SI, McNaughton BL. Comparison of spatial firing characteristics of units in dorsal and ventral hippocampus of the rat. *J Neurosci*. 1994:14:7347–7356.

Kahn I, Andrews-Hanna JR, Vincent JL, Snyder AZ, Buckner RL. Distinct cortical anatomy linked to subregions of the medial temporal lobe revealed by intrinsic functional connectivity. *J Neurophysiol*. 2008:100:129–139.

Killian NJ, Jutras MJ, Buffalo EA. A map of visual space in the primate entorhinal cortex. *Nature*. 2012:491:761–764.

Kim H. *Hippocampus*. 2015:25:500–510. https://doi.org/10.1002/hipo.22387.

Kjelstrup KB, Solstad T, Brun VH, Hafting T, Leutgeb S, Witter MP, Moser EI, Moser MB. Finite scale of spatial representation in the hippocampus. *Science*. 2008:80-). 321:140–143.

Komorowski RW, Garcia CG, Wilson A, Hattori S, Howard MW, Eichenbaum H. Ventral hippocampal neurons are shaped by experience to represent behaviorally relevant contexts. *J Neurosci*. 2013:33:8079–8087.

Levine B, Svoboda E, Hay JF, Winocur G, Moscovitch M. Aging and autobiographical memory: dissociating episodic from semantic retrieval. *Psychol Aging*. 2002:17:677–689.

Logothetis NK, Pauls J, Augath M, Trinath T, Oeltermann A. Neurophysiological investigation of the basis of the fMRI signal. *Nature*. 2001:412:150–157.

Lubenov EV, Siapas AG. Hippocampal theta oscillations are travelling waves. *Nature*. 2009:459(7246):534–539.

MATLAB. *9.7.0.1190202 (R2019b)*. Natick, Massachusetts: The MathWorks Inc; 2018.

Poppenk J, Moscovitch M. A hippocampal marker of recollection memory ability among healthy young adults: contributions of posterior and anterior segments. *Neuron*. 2011:72: 931–937.

Poppenk J, Evensmoen HR, Moscovitch M, Nadel L. Long-axis specialization of the human hippocampus. *Trends Cogn Sci*. 2013:17: 230–240.

Quiroga QR. Plugging in to human memory: advantages, challenges, and insights from human single-neuron recordings. *Cell*. 2019:179(5):1015–1032.

Raghunathan TE, Rosenthal R, Rubin DB. Comparing correlated but nonoverlapping correlations. *Psychol Methods*. 1996:1:178–183.

Ritchey M, Libby LA, Ranganath C. *Cortico-hippocampal systems involved in memory and cognition: the PMAT framework*. 1st ed. Progress in Brain Research. Elsevier B.V; 2015

Robin J, Moscovitch M. Details, gist and schema: hippocampal-neocortical interactions underlying recent and remote episodic and spatial memory. *Curr Opin Behav Sci*. 2017:17:114–123.

Schacter DL, Wagner AD. Medial temporal lobe activations in fMRI and PET studies of episodic encoding and retrieval. *Hippocampus*. 1999:9:7–24.

Smith SM, Jenkinson M, Woolrich MW, Beckmann CF, Behrens TEJ, Johansen-Berg H, Bannister PR, De Luca M, Drobnjak I, Flitney DE, et al. Advances in functional and structural MR image analysis and implementation as FSL. *NeuroImage*. 2004:23(Suppl 1): S208–S219.

Spitmaan M, Seo H, Lee D, Soltani A. Multiple timescales of neural dynamics and integration of task-relevant signals across cortex. *Proc Natl Acad Sci U S A*. 2020:117:22522–22531.

Strange BA, Witter MP, Lein ES, Moser EI. Functional organization of the hippocampal longitudinal axis. *Nat Rev Neurosci*. 2014:15: 655–669.

Tambini A, Davachi L. Persistence of hippocampal multivoxel patterns into postencoding rest is related to memory. *Proc Natl Acad Sci U S A*. 2013:110:19591–19596.

Thakral PP, Madore KP, Kalinowski SE, Schacter DL. Modulation of hippocampal brain networks produces changes in episodic simulation and divergent thinking. *Proc Natl Acad Sci U S A*. 2020:117: 12729–12740.

Vanni S, Sharifian F, Heikkinen H, Vigário R. Modeling fMRI signals can provide insights into neural processing in the cerebral cortex. *J Neurophysiol*. 2015:114:768–780.

Wagner AD, Shannon BJ, Kahn I, Buckner RL. Parietal lobe contributions to episodic memory retrieval. *Trends Cogn Sci*. 2005:9: 445–453.

Wang JX, Rogers LM, Gross EZ, Ryals AJ, Dokucu ME, Brandstatt KL, Hermiller MS, Voss JL. Memory enhancement: targeted enhancement of cortical-hippocampal brain networks and associative memory. *Science (80-)*. 2014:345:1054–1057.

Wickramaarachchi C, Frincu M, Small P, Prasanna VK. Fast parallel algorithm for unfolding of communities in large graphs. *2014 IEEE High Perform Extrem Comput Conf HPEC*. Waltham, MA, USA: IEEE Institute of Electrical and Electronics Engineers; 2014.

Wu X, Yang W, Tong D, Sun J, Chen Q, Wei D, Zhang Q, Zhang M, Qiu J. A meta-analysis of neuroimaging studies on divergent thinking using activation likelihood estimation. *Hum Brain Mapp*. 2015:36: 2703–2718.

Zhang H, Fell J, Axmacher N. Electrophysiological mechanisms of human memory consolidation. *Nat Commun*. 2018:9:4103. https://doi.org/10.1038/s41467-018-06553-y.